Effect of organic solvents on the kinetics of reversible inclusion of palmatine in cucurbit[7]uril

Mónika Megyesi, Zsombor Miskolczy, László Biczók*

Institute of Materials and Environmental Chemistry, HUN-REN Research Centre for Natural Sciences, P.O. Box 286, 1519 Budapest, Hungary

* Corresponding author. E-mail: biczok.laszlo@ttk.hu

Abstract

The effects of the organic cosolvents methylformamide (MF), dimethylformamide (DMF), dimethyl sulfoxide (DMSO), and acetonitrile (AN) on the reversible inclusion of the natural alkaloid palmatine (Pal) in cucurbit[7]uril (CB7) were investigated using fluorescence spectroscopy, stopped-flow measurements, and isothermal titration calorimetry. Kinetic studies revealed that cosolvents not only compete with Pal for CB7 binding but also modulate both the formation and dissociation rates of Pal–CB7 complex. Cosolvent confinement in CB7 was exothermic, with dimethylformamide showing the strongest affinity due to the favorable entropic contribution to the driving force. Even small cosolvents fractions reduced the enthalpy gain of Pal–CB7 formation, which was partly compensated by entropy increases in the presence of methylformamide, acetonitrile, and dimethyl sulfoxide. Direct monitoring of the complex dissociation demonstrated cosolvent-promoted acceleration of Pal release, driven by a greater decrease in activation enthalpy than activation entropy. Dimethylformamide addition enhanced the rate of Pal association with CB7, acetonitrile exerted negligible influence, whereas dimethyl sulfoxide and methylformamide slowed the process. These results underscore the essential role of cosolvent-induced perturbations in the hydrogen-bonded water network and solvation shell in modulating both thermodynamics and kinetics of host–guest complexation.

Keywords: host-guest complex; activation parameters, solvent effect, water structure, binding constant

1. Introduction

Organic cosolvents are widely used as solubilizing excipients in water-based pharmaceutical formulations [1, 2] and for tuning the properties of aqueous polymer solutions [3, 4]. They affect the stability and conformational dynamics of proteins [5], induce morphological transformations in self-assembled polypeptides [6], and regulate the catalytic activities of enzymes [7, 8]. A deoxyribozyme capable of RNA-cleaving only in the presence of DMSO has been developed [9]. Cosolvent-driven chiral inversion has been achieved in self-assembled peptides and one-dimensional coordination polymers [10, 11]. Even trace amounts of organic solvents can direct and mediate dipeptide self-assembly in aqueous media [12].

Due to their inclusion complex formation, water-soluble macrocyclic compounds have diverse applications in biomedical field [13], chemical sensing [14], catalysis [15], material science [16], and separation technologies [17]. Their binding affinity and the properties of their host-guest complexes can be effectively modulated by cosolvents. The combined use of cosolvents and cyclodextrins (CDs), a family of cyclic oligosaccharides composed of glucopyranose units, has been investigated to achieve an optimized synergistic effect [18-20]. Increasing the concentration of ethanol or dimethyl sulfoxide (DMSO) in aqueous solution reduced the stability of CD complexes by decreasing the exothermicity of their formation [21, 22]. Combined molecular dynamics and NMR studies demonstrated the competitive inclusion of propiconazole nitrate and DMSO in β-cyclodextrin, along with a decrease in guest binding affinity with increasing DMSO volume fraction in water [23].

Despite the diverse potential applications of the pumpkin-shaped cucurbit[n]uril cavitands [24, 25], little information is available on their inclusion complex formation in water–cosolvent mixtures. NMR spectroscopic experiments with a few organic solvents showed 1:1 incorporation into cucurbit[7]uril (CB7) and provided the binding constants of the resulting complexes [26]. The addition of 4 vol% ethanol to an aqueous solution of CB7-encapsulated

48 palmatine or dehydrocorydaline resulted in a less than 10-fold reduction in the binding constant,
49 whereas akali chlorides produced a more pronounced effect [27]. Isothermal calorimetric
50 titrations revealed that the driving force of 2',2'-difluoro-2'-deoxycytidine anticancer drug
51 confinement in CB7 was reduced with increasing ethanol mass fraction in aqueous formate
52 buffer because the decrease in enthalpy release was not compensated for the enhanced entropy
53 gain [28]. The presence of 4 vol% methanol weakened the rhodamine B binding in CB7 and 4-
54 sulfonatocalix[4]arene, but improved the complexation ability of β-cyclodextrin [29]. In
55 contrast, the addition of 20 vol% methanol did not significantly affect the stability of the oxime–
56 CB7 complexes in aqueous solutions, but the same amount of acetonitrile (AN) caused a
57 decrease in the binding constant by almost two orders of magnitude [30]. Masson and coworker
58 demonstrated that the addition of 40 vol% CD_3CN to the solution of the 2:2 cucurbit[8]uril
59 (CB8) complexes of platinum(II) terpyridyl acetylide derivatives in D_2O triggered the release
60 of one CB8 macrocycle and the reorientation of the guests into a stacked head-to-head direction
61 in the remaining 2:1 complexes [31]. The change in solvent from water to dimethyl sulfoxide
62 (DMSO) caused cation-induced trimerization of the CB7 inclusion complexes [32]. A
63 remarkable solvent effect was also observed for the interaction mode between the diheptyl-4,4'-
64 bipyridinium dication and CB7. The aromatic rings of the guest were encapsulated in DMSO,
65 whereas the heptyl chain was included in the host cavity when water was used as a solvent [33].
66 Different moieties of N-substituted 4-benzoylpyridinium cations were embedded into CB7 in
67 water and DMSO, but the binding constants were less than one order of magnitude smaller in
68 the latter [34]. The one-electron oxidation of the (ferrocenylmethyl)trimethylammonium cation
69 enhanced its affinity for CB7 in AN and DMSO, but the opposite effect was observed in water
70 [35]. Dumbbell-shaped guests formed rotaxane-like complexes with CB7 through
71 thermodynamically more favorable and substantially faster processes in aqueous media than in
72 DMSO [36].

Despite the great potential of water–organic solvent binary mixtures in the design of tailor-made functional CB*n*-based systems, no systematic studies have been performed to reveal the molecular details of the cosolvent effect on the kinetics and thermodynamics of CB*n* complex formation. To fill this knowledge gap, we systematically investigated the complex formation of palmatine (Pal) natural alkaloid with CB7 (Scheme 1) in aqueous solutions

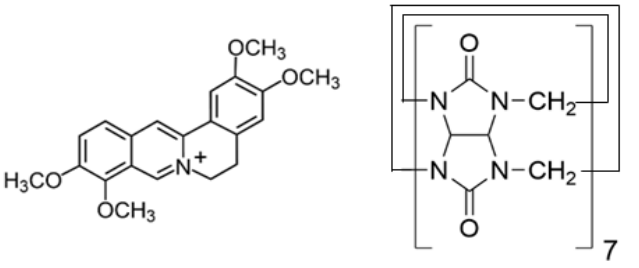

palmatine (Pal) cucurbit[7]uril (CB7)

Scheme 1 Chemical structures of the host and guest compounds

containing DMSO, AN, dimethyl formamide (DMF), or methyl formamide (MF). Pal was selected as a model compound owing to its several advantageous properties: (a) it exhibits strong fluorescence inside the nonpolar cavity of CB7 but has a negligible emission in water, enabling the direct monitoring of inclusion complex formation; (b) it binds to CB7 with high affinity, providing a broad range to assess cosolvent-induced reductions in binding constant; (c) it does not undergo in acid−base reactions that could complicate the evaluation of cosolvent effects; (d) the high fluorescence quantum yield of its CB7 complex permits the use of very dilute solutions, thereby slowing down the bimolecular processes; and (e) its ingress into and egress from CB7 take place within a conveniently measurable timescale. The cosolvents were selected based on their distinct effect on water structure. DMF strengthens the hydrogen bond network of water [37]. At concentrations below 1.4 vol%, AN occupies the pre-existing cavities of the water structure and reduces the number of water-water hydrogen bonds [38], while DMSO [39] and MF [40] markedly disrupt the hydrogen-bond network of water. Our aim was to assess whether such cosolvent-induced modifications of water structure play a decisive role

in governing the kinetics of reversible formation of Pal–CB7 inclusion complex. We also intended to investigate the effect of guest size. Calculations showed that the volume of the cosolvent molecules gradually increases in the order AN < MF < DMSO < DMF. DMSO was included among the selected cosolvents because of its widespread use in biological research and its role as a cryoprotectant [41, 42].

2. Materials and methods

2.1. Reagents

Palmatine chloride (Pal, ≥98% Sigma-Aldrich) was purified by chromatography using a silica gel (Merck) column and ethanol eluent. High-purity CB7 was provided by Dr. Anthony I. Day (University of New South Wales, Canberra, Australia). 1-Adamantylamine hydrochloride (Sigma-Aldrich), 5-chloro-2-adamantanone (98 %, TCI), bis(cyclopentadienyl)cobalt(III) hexafluorophosphate (96 %, TCI), and organic solvents (Merck) were used as received. Water was distilled twice from the dilute $KMnO_4$ (VWR International) solution.

2.2. Spectroscopic measurements

The absorption and corrected fluorescence spectra were recorded using a Cary60 spectrophotometer (Agilent Technologies, Santa Clara, CA, USA) and a Fluoromax-4 spectrofluorometer (Jobin-Yvon, Longjumeau, France), respectively. The binding constants for 1:1 complex formation (K) were calculated by analyzing the total CB7 concentration ($[CB7]_0$) dependence of the fluorescence intensity (I) at a specific wavelength using the following equation [43]:

$$I = I_0 + \frac{I_\infty - I_0}{2}\left\{1 + \frac{[CB7]_0}{[Pal]_0} + \frac{1}{K[Pal]_0} - \left[\left(1 + \frac{[CB7]_0}{[Pal]_0} + \frac{1}{K[Pal]_0}\right)^2 - 4\frac{[\mathrm{CB7}]_0}{[Pal]_0}\right]^{\frac{1}{2}}\right\} \quad (1)$$

where $[Pal]_0$ is the total Pal concentration, I_∞ and I_0 represent the fluorescence intensities of the fully complexed and free Pal. $[Pal]_0$ = 1 μM was typically used.

Fluorescence quantum yields (Φ_f) were determined relative to that of quinine sulfate in a 0.5 M H_2SO_4 solution, for which a reference yield of $\Phi_{ref} = 0.546$ was taken [44]. The samples were excited at 360 nm, where the absorbances were A and A_{ref} for the sample and reference solutions, respectively. To avoid inner filter effect, the absorbance of the samples was adjusted to approximately 0.1 at 360 nm. The Φ_f values were calculated based on the following relationship [43]:

$$\Phi_f = \Phi_{ref} \frac{I(1-10^{-A_{ref}})}{I_{ref}(1-10^{-A})} \left(\frac{n}{n_{ref}}\right)^2 \quad (2)$$

I and I_{ref} are the integrals of the corrected fluorescence spectra, while n and n_{ref} denote the refractive indices of the sample and reference solutions, respectively. Table S1 in the Supplementary data lists the previously published refractive indices [38, 45-47] used for the calculations. To obtain the I value of the fully complexed Pal, the measured fluorescence intensity integrals were extrapolated to complete complexation using the Pal–CB7 binding constants ($K_{1:1}$) obtained from separate experiments (vide infra).

Fluorescence lifetimes (τ_f) were measured by the time-correlated single-photon counting method, as described previously [48]. A Picoquant diode laser (pulse duration ca. 70 ps, wavelength 372 nm) excited the samples, and the temporal decay of the fluorescence intensity was fitted using the nonlinear least-squares reconvolution method with the Picoquant FluoFit software.

2.3. Stopped-flow kinetics

The formation and dissociation of the Pal–CB7 complex were studied using stopped-flow method with a Fluoromax-4 spectrofluorometer equipped with an Applied Photophysics RX2000 rapid mixing accessory and a pneumatic drive. The temperature control was maintained with a Julabo F25-ED thermostat. The time resolution was set to 20 ms/channel.

145 For each measurement, 10–20 kinetic traces were averaged, and the data were analyzed using
146 homemade programs written in MATLAB 7.9. To slow the rapid bimolecular host-guest
147 association to a timescale accessible to the stopped-flow technique, low concentrations of Pal
148 and CB7 (typically ~0.25 μM) were used in kinetic studies. Owing to the high sensitivity of the
149 fluorescence detection and the high fluorescence quantum yield of the Pal–CB7 complex,
150 excellent signal-to-noise ratios were achieved under these experimental conditions.
151
152 *2.4 Isothermal titration calorimetry (ITC)*
153 Isothermal calorimetric titrations were performed with a VP-ITC (GE Healthcare,
154 Chicago, IL, USA) instrument at 298 K. All solutions were degassed prior to titration. Proper
155 mixing was ensured by stirring at 307 rpm allowing 300 s intervals between successive
156 additions. Because calorimetry is inherently much less sensitive than fluorescence detection,
157 higher host and guest concentrations were required in the ITC experiments than in the other
158 measurements. The reactant concentrations, injected volumes, and injection durations were
159 adjusted to ensure optimal experimental conditions. First, the enthalpy gain associated with
160 cosolvent–CB7 complexation was determined by stepwise injections of 40 μL CB7 solution
161 (0.4 mM, injection duration 40 s) from a computer-controlled microsyringe into a 0.2 M
162 aqueous cosolvent solution. The integrated heat released per injection is a directly measured
163 quantity that does not depend on any assumptions regarding the stoichiometry and binding
164 constant of complexation. The measured enthalpy change was corrected for the heat released
165 upon the addition of the same volume of water and for the minor enthalpy change detected upon
166 injecting 40 μL CB7 solution (0.4 mM) into water. The corrected enthalpy change (ΔH_{CORR})
167 was then extrapolated to the complete cosolvent–CB7 complex formation, taking into account
168 the bound fraction of CB7 (α), assuming 1:1 complexation, as follows:

169 $$\Delta H_{\mathrm{CS}} = \frac{\Delta H_{\mathrm{CORR}}}{\alpha} = \Delta H_{\mathrm{CORR}} \frac{1+K_{\mathrm{CS}}[\mathrm{cosolvent}]}{K_{\mathrm{CS}}[\mathrm{cosolvent}]} \quad (3)$$

where K_{CS} is the binding constant of cosolvent–CB7 complexation obtained from independent ITC experiments described in the next paragraph (K_{CS} values are listed in Table 1). The ΔH_{CS} values were derived from the first six injections, where the contribution of multiple binding is expected to be small. These ΔH_{CS} values were then averaged to obtain the final results.

In the second step, the experimental parameters were optimized to ensure accurate determination of the K_{CS} values. Aqueous CB7 solutions (0.55–0.72 mM) were titrated with aqueous solutions of 21.4 mM DMF, 74.7 mM DMSO, 989 mM MF, or 1000 mM AN. The titrant concentrations were changed to account for the differing binding affinities of the cosolvents. The dilution heat, determined by titrating the cosolvents into water under identical conditions, was subtracted from the enthalpograms. The resulting data were then analyzed with a single set of identical sites model, while keeping the corresponding ΔH_{CS} values from the first experimental series fixed. This procedure reduced the number of unknown parameters, yielding more accurate K_{CS} values and binding stoichiometries (N). Here, N denotes the mean number of guest molecules accommodated by the host macrocycle. The Gibbs free energy (ΔG_{CS}), and entropy changes (ΔS_{CS}) upon cosolvent complexation with CB7 were calculated according to the well-established thermodynamic relationships:

$$\Delta G_{CS} = -RT \ln K_{CS} \quad (4)$$

$$\Delta S_{CS} = \Delta H_{CS}/T + R \ln K_{CS} \quad (5)$$

where T is the absolute temperature, and R is the universal gas constant.

When the thermodynamic parameters of Pal–CB7 complex formation were determined in 0.2 M cosolvent aqueous solutions, the titrand and titrant solutions contained 33.0 - 43 μM CB7 and ~420 μM Pal, respectively.

2.5 Calculation of molecular volumes and packing coefficients

The energy-minimized structures of the cosolvents were obtained using the RM1 semiempirical method implemented in HyperChem 8.0 (Hypercube, Inc.). The molecular

volumes of the optimized geometries were subsequently calculated with the QSAR module of the same program. For the inner cavity volume of CB7, a value of 242 Å³ was used, as recommended by Nau and co-workers [49]. The packing coefficients (PC) of the cosolvents were determined as the ratio of the guest molecular volume to the host cavity volume.

2.6 Data statistical analysis

Each experiment was repeated at least three times, and the reported errors correspond to the standard deviations of the measured values.

3. Results

3.1. Study of organic cosolvent inclusion in CB7 by isothermal titration calorimetry (ITC)

NMR studies and molecular mechanics calculations have demonstrated the inclusion of organic solvents in CB7 cavity, and 1:1 association has been proposed [26]. To elucidate the enthalpy gain associated with the complexation (ΔH_{CS}), we performed isothermal titration calorimetry

Table 1 Molecular volumes and packing coefficients of cosolvents, along with the stoichiometric and thermodynamic parameters of their CB7 complexes in water at 298 K, derived from ITC data analyzed with the single set of identical sites binding model.

	Cosolvent			
	MF	DMSO	AN	DMF
Volume / Å^3	59	69	47	76
PC / %	24	29	19	31
N	0.90 ± 0.10	0.94 ± 0.08	2.08 ± 0.09	1.04 ± 0.05
K_{CS} / M^{-1}	16 ± 1	166 ± 10	6 ± 2	1070 ± 100
ΔG_{CS} / kJ mol^{-1}	–6.9 ± 0.3	–12.7 ± 0.2	–4.4 ± 0.9	–17.3 ± 0.3
ΔH_{CS} / kJ mol^{-1}	–17.8 ± 1.2	–18.5 ± 1.3	–11.8 ± 1.3	–13.6 ± 1.3
ΔS_{CS} / J mol^{-1} K^{-1}	–36 ± 4	–20 ± 4	–24 ± 4	12 ± 4

(ITC) measurements, as detailed in the Materials and methods section. The results are presented in Fig. S1 in the Supplementary data, and the mean values of the calculated ΔH_{CS} are reported in Table 1. Dilution of a 0.4 mM CB7 aqueous solution produced negligible heat effect. The enthalpy change observed upon the addition of water to the 0.2 M aqueous cosolvent solution was always smaller than the enthalpy decrease associated with cosolvent–CB7 complexation.

After the accurate determination of ΔH_{CS} values, the reactant concentrations were optimized for the determination of the binding constants (K_{CS}) and the mean number of

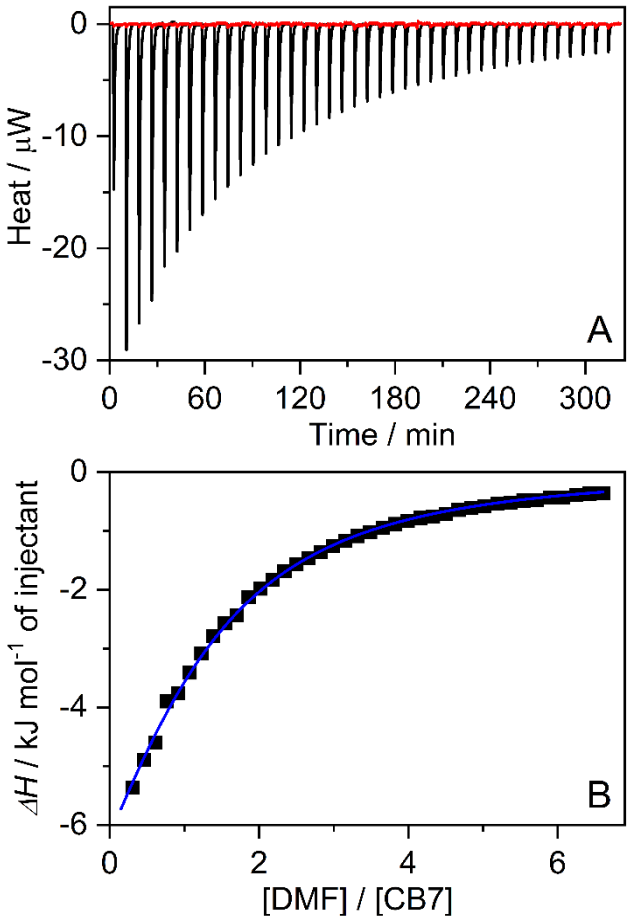

Fig. 1. (A) Heat release upon sequential injections of 7 μL of 21.4 mM DMF solution into of 0.695 mM CB7 in water at 298 K (injection duration: 14 s). Red line shows the dilution heat obtained by the injection of DMF solution into water. (B) The integrated heat released per injection, after subtraction of the dilution heat of DMF (■), is plotted as a function of the [DMF]/[CB7] molar ratio. The line represents the best fit obtained using the single set of identical sites model.

cosolvent molecules in CB7 (N). Fig. 1 displays a representative enthalpogram recorded during the stepwise addition of 21.4 mM DMF aqueous solution to 0.695 mM CB7 in water at 298 K, while the results of analogous ITC experiments with the other cosolvents are presented in Figs. S2–S4. The binding constants (K_{CS}) and stoichiometric parameters (N) for the host-guest complexations were obtained from the nonlinear least-squares fitting of the ITC data. Owing to the strong correlation between ΔH_{CS} and N, the ΔH_{CS} parameter was fixed to the value obtained from the independent experiments described above. For the DMF, DMSO, and MF cosolvents, the data were well described by the 1:1 encapsulation model, as evidenced by N values close to unity (Table 1). In contrast, the confinement of AN in CB7 yielded an N value of 2, consistent with the small size and low packing coefficient (PC) of this cosolvent, indicating that two AN molecules can be included in CB7. The single set of identical sites binding model used here assumes that CB7 accommodates N molecules of AN with the same binding constant (K_{CS}) and binding enthalpy ΔH_{CS}. Alternative models that distinguish between the thermodynamic parameters of 1:1 and 2:1 complexes were not applicable because they introduce too many adjustable parameters for reliable fitting.

The results of ITC measurements summarized in Table 1 demonstrate that the weak affinity of AN for CB7 originates primarily from the low exothermicity of their interaction, whereas the effective binding of DMF to CB7 is driven largely by the substantial entropic contribution to the driving force of association. Among the studied cosolvents, only DMF encapsulation in CB7 is accompanied by an entropy gain. The determined K_{CS} values are consistent, within experimental error, with those obtained from ^{1}H NMR chemical shift titrations for AN (11 ± 1 M^{-1}), DMSO (140 ± 20 M^{-1}) and DMF (1000 ± 80 M^{-1}) [26] and exhibit a parallel increase with the packing coefficients, defined as the ratio of the guest's molecular volume to the inner cavity volume of CB7 [50].

253 *3.2. Characterization of the Pal–CB7 complex in equivolume water–cosolvent mixtures*

254 Pal can act as a fluorescent probe for its surroundings [51-53]. Taking advantage of this
255 ability, the photophysical characteristics of the Pal–CB7 complex were examined in 1:1 (v/v)
256 water–cosolvent mixtures to assess whether the microenvironment of the CB7-encapsulated Pal
257 changed upon cosolvent addition. The fluorescence lifetime of Pal–CB7 (τ_f = 11.6 ns in water)
258 was only negligibly affected by the presence of cosolvents (Table 2). The fluorescence quantum
259

260 **Table 2** Binding constants and photophysical parameters of Pal–CB7 complex in water and 1:1
261 (v/v) water–cosolvent mixtures

	H_2O [a]	1:1 (v/v) water–cosolvent mixture			
		MF	DMSO	AN	DMF
$K_{1:1}$ / 10^3 M^{-1}	26000 ± 3000[b]	3.6 ± 0.2	25 ± 2	0.88 ± 0.14	1.6 ± 0.2
τ_f / ns	11.7 ± 0.3	12.1 ± 0.3	12.1 ± 0.3	11.9 ± 0.3	11.5 ± 0.3
Φ_f	0.26 ± 0.02	0.23 ± 0.02	0.31 ± 0.03	0.23 ± 0.02	0.14 ± 0.02
k_f / 10^7 s^{-1}	2.2 ± 0.2	1.9 ± 0.2	2.6 ± 0.3	1.9 ± 0.2	1.2 ± 0.2
k_{nr} / 10^7 s^{-1}	6.3 ± 0.3	6.4 ± 0.3	5.7 ± 0.3	6.5 ± 0.3	7.5 ± 0.3

262 [a] in the absence of cosolvent, [b] reference [54]

263

264 yields (Φ_f), determined using equation (2), varied slightly, mainly because of changes in the
265 radiative rate constants (k_f). The rate constants for the radiative and nonradiative energy
266 dissipation processes were derived using the relationships $k_f = \Phi_f/\tau_f$ and $k_{nr} = (1-\Phi_f)/\tau_f$,
267 respectively [43]. According to the Strickler–Berg equation [55], k_f depends on the refractive
268 index of the medium, the integral over the first absorption band, and the mean fluorescence
269 frequency. The insignificant changes in τ_f indicate that the cosolvents do not alter the
270 microenvironment experienced by Pal when encapsulated within the CB7 cavity.

271 The binding constant for Pal incorporation into CB7 was also determined in 1:1 (v/v)
272 water–cosolvent mixtures. Fig. S5 displays the variation of normalized fluorescence intensity

of 1 μM Pal solutions with CB7 concentration. Fitting equation (1) to the experimental data provided the binding constants summarized in Table 2. Among the tested cosolvents, Pal exhibited the highest binding constant ($K_{1:1}$) in the water–DMSO mixture, with an identical value obtained in neat DMSO (Fig. S6 in the Supplementary data). In contrast, fluorescence titration in neat MF (Fig. S7 in the Supplementary data) yielded a binding constant of (1.1 ± 0.1)×10^3 M^{-1}, which is approximately threefold lower than that measured in the 1:1 (v/v) water–MF mixture. The low CB7 solubility thwarted the complexation in neat DMF and AN.

No correlation was found between the inclusion propensity of the cosolvents in CB7 (K_{CS}, Table 1) and their impact on Pal–CB7 complexation ($K_{1:1}$, Table 2). Pal showed the weakest affinity to CB7 in the water–AN mixture (Table 2), despite the low propensity of AN to be encapsulated by CB7. Furthermore, AN diminished the inclusion ability of Pal more strongly than DMSO, even though DMSO had a larger K_{CS} value. These findings suggest that cosolvents reduce the inclusion efficiency of Pal not only through direct competition for the host cavity, but also via additional contributing factors.

3.3. Pal–CB7 complex formation in the presence of 0.2 M cosolvents

To minimize the influence of bulk solvent polarity change, Pal–CB7 complex formation was also studied in dilute (0.2 M) cosolvent solutions, corresponding to ~1–1.5 vol% concentrations. Under these conditions, the ITC experiments showed a decrease in K in the order AN > MF > DMSO > DMF (Table 3), which contrasts sharply with the trend observed in 1:1 (v/v) water-cosolvent mixtures (Table 2, DMSO > MF > DMF > AN). This discrepancy clearly indicates that the cosolvent-induced modifications of the water structure govern the binding propensity of Pal in CB7, as variations in cosolvent concentration perturb the hydrogen-bonded network of water to different extents and in distinct manners.

Table 3 Binding constants and thermodynamic parameters obtained from ITC measurements, along with the kinetic parameters of the Pal–CB7 complex in water and in 0.2 M cosolvent aqueous solutions at 298 K.

	H_2O [a]	0.2 M Cosolvent			
		MF	DMSO	AN	DMF
N		0.92 ± 0.08	0.96 ± 0.08	0.98 ± 0.08	0.92 ± 0.08
K/ 10^5 M^{-1}	260 ± 30	13 ± 1	7.5 ± 1.3	22 ± 2	0.91 ± 0.10
k_{in}/k_{out} /10^5 M^{-1}	270 ± 30	14.2 ± 0.9	8.1 ± 0.8	22.6 ± 0.9	[b]
ΔG / kJ mol^{-1}	–42.3 ± 0.3	–34.9 ± 0.2	–33.5 ± 0.4	–36.2 ± 0.2	–28.3 ± 0.3
ΔH / kJ mol^{-1}	–37 ± 2	–28.0 ± 0.7	–23.7 ± 0.5	–22.8 ± 1.0	–31.6 ± 0.9
ΔS / J mol^{-1} K^{-1}	9 ± 4	23 ± 3	33 ± 2	45 ± 4	–11 ± 3
k_{out}(slope) / M^{-1} s^{-1}		1.8 ± 0.1	4.1 ± 0.2	9.0 ± 0.4	55 ± 1
$\Delta H^{‡}_{out}$ / kJ mol^{-1}	76.8 ± 2.0	65.3 ± 2.0	62.4 ± 2.0	59.2 ± 2.0	52.1 ± 2.0
$\Delta S^{‡}_{out}$ / J mol^{-1} K^{-1}	2 ± 1	–30 ± 4	–35 ± 4	–40 ± 4	–50 ± 4
$\Delta G^{‡}_{out}$ / kJ mol^{-1}	76.2 ± 2.0	74.2 ± 2.3	72.8 ± 2.3	71.1 ± 2.3	67.0 ± 2.3

[a] in the absence of cosolvent [54], [b] cannot be measured at 0.2 M concentration

To reveal how cosolvents alter the thermodynamics of Pal–CB7 complex formation, isothermal titration calorimetry measurements were performed at 298 K. Both reactants were dissolved in 0.2 M cosolvents aqueous solution. The amount of heat evolved after each addition of Pal to the CB7 solution was corrected with the dilution heat obtained by Pal injection into the solvent. Figs. S8-S11 in the Supplementary data present representative enthalpograms, and the results of the nonlinear least-squares fits using the single set of identical sites model are summarized in Table 3. The exothermicity of the complexation (ΔH) was markedly reduced by the presence of each cosolvent. However, ΔH considerably varied among cosolvents, reflecting their district effect on the solvent structure change. Interestingly, entropy loss upon Pal–CB7 formation was found only in the presence of DMF, which is known to strengthen the hydrogen bond network of water [37]. In contrast, the other cosolvents used in the present studies enhanced the entropy gain relative to that observed in neat water.

315 *3.4. Kinetics of Pal exit from CB7 in cosolvent–water mixtures*

316 To elucidate the origin of the cosolvent effects on host–guest association, the dissociation
317 kinetics of the Pal–CB7 complex was investigated using stopped-flow fluorescence
318 measurements. Because only encapsulated Pal fluoresced intensely, changes in emission
319 directly tracked the Pal–CB7 concentration. The Pal egression rate constant was determined
320 separately, as described previously [56]. Rapid 1:1 mixing of an equimolar (~0.5 μM) Pal and
321 CB7 solution with 1-adamantylammonium (AH^+, 10 μM) induced Pal release, with AH^+ swiftly
322 occupying the vacated CB7 cavity. Negligible AH^+–CB7 dissociation on the experimental
323 timescale prevented the reformation of Pal–CB7. Thus, the observed fluorescence decay
324 exclusively reflected Pal–CB7 dissociation. The Supplementary data (Figs. S12-S15) provide
325 evidence for the high binding constant of AH^+–CB7, even in the presence of a cosolvent,
326 resulting in negligible dissociation under our experimental conditions.

327 Fig. 2 shows that even a small amount of cosolvent substantially altered the rate of Pal
328 release from CB7. The fluorescence decays were recorded after rapid mixing of equimolar Pal

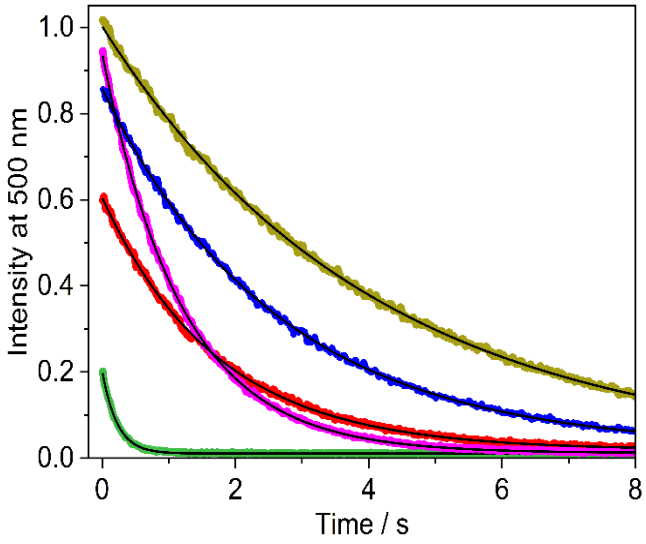

329 **Fig. 2** Temporal decay of the fluorescence intensity in water (—), in the presence of 76 mM
330 AN (—), 84 mM MF (—), 84 mM DMSO (—), and 83 mM DMF (—) after mixing equimolar
331 Pal and CB7 solutions with AH^+ solution. Excitation occurred at 340 nm, [Pal] = [CB7] = 0.25
332 μM, and [AH^+] = 5 μM at t = 0 s.

and CB7 solutions with AH^+ solution in the presence of various cosolvents. The initial intensities (I_0) decreased because a smaller fraction of Pal was complexed in that cosolvent-containing solutions than in neat water owing to competitive binding. The addition of the cosolvent also modified the exponential decay rates, indicating effects beyond simple competition. Fitting the decays to a single-exponential function ($I = I_\infty + I_0 \exp(-k_{out}t)$ yielded the rate constant for the Pal egression (k_{out}) from the CB7 cavity. Similar experiments were conducted in the presence of varying amounts of cosolvents (Figs. S16-S19 in the Supplementary data). The rate constant k_{out} increased linearly with the cosolvent concentration (Fig. 3A), as described by the following equation:

$$k_{out} = k_{out}^{HD} + k_{out}(\text{slope})[\text{cosolvent}] \quad (6)$$

The intercept corresponds to the rate constant of Pal–CB7 dissociation in water (k_{out}^{HD}), which agrees well with the previously reported value of $k_{out}^{HD} = 0.20 \pm 0.04$ s^{-1} [54, 57]. The slopes (k_{out}(slopes)) increased markedly in the order of MF < DMSO < AN < DMF (Table 3). This is an unexpected finding, as k_{out} should remain independent of cosolvent concentration if only competitive binding to CB7 takes place. The parallel cosolvent–CB7 complex formation equilibrium does not affect the spontaneous unimolecular Pal release from CB7. Enhancement of k_{out} may arise from cosolvent-induced changes in the water structure, from a bimolecular reaction of the cosolvent with Pal–CB7, or from the formation of a ternary Pal–CB7–cosolvent complex.

To obtain a deeper understanding of the substantial increase in k_{out}, temperature-dependent measurements were performed at a 0.2 M cosolvent concentration, where Pal egression remained within the measurable range even for DMF at 298 K. The aforementioned k_{out} measurements were repeated at various temperatures (T) in the presence of different cosolvents and, for comparison, in pure water. The Arrhenius plots of these results are presented in Figure 3B. The pre-exponential factor (A_{out}) and activation energy (E_{out}) of the

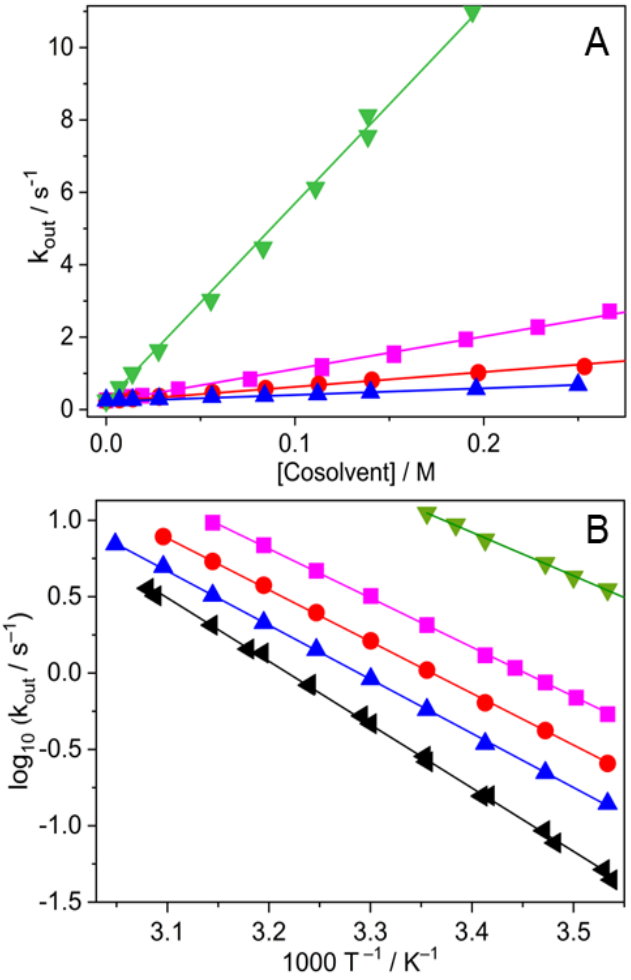

Fig. 3 (A) Rate constants for the Pal exit from CB7 as a function of cosolvent concentration in water at 298 K. (B) Arrhenius plots of the egression rate constants in water (◀) and in 0.2 M cosolvent aqueous solution; DMF (▼), AN (■), DMSO (●), and MF (▲).

cosolvent-promoted Pal exit from CB7 were obtained by nonlinear least-squares fitting of the temperature dependence of k_{out} with the Arrhenius equation

$$k_{out} = A_{out} \exp(-E_{out}/RT) \quad (7)$$

where R is the universal gas constant. According to transition-state theory, the standard enthalpy ($\Delta H^{\ddagger}_{out}$), entropy ($\Delta S^{\ddagger}_{out}$), and Gibb's free energy ($\Delta G^{\ddagger}_{out}$) of activation were derived as follows [54]:

$$\Delta H^{\ddagger}_{out} = E_{out} - RT \quad (8)$$

$$\Delta S^{\ddagger}_{\mathrm{out}} = \mathrm{R}\ln\left(A_{\mathrm{out}}\frac{\mathrm{h}}{\kappa \mathrm{e} \mathrm{k}_{\mathrm{B}} T}\right) \quad (9)$$

$$\Delta G^{\ddagger}_{\mathrm{out}} = \Delta H^{\ddagger}_{\mathrm{out}} - T\Delta S^{\ddagger}_{\mathrm{out}} \quad (10)$$

where e is the base of the natural logarithm, k_B represents the Boltzmann constant, h stands for the Planck constant, and the transmission coefficient (κ) was assumed to be unity. The calculated activation parameters are summarized in Table 3. Both $\Delta H^{\ddagger}_{\mathrm{out}}$ and $\Delta S^{\ddagger}_{\mathrm{out}}$ decreased considerably upon the addition of 0.2 M cosolvent, following the order MF > DMSO > AN > DMF.

3.5. Kinetics of Pal entry into CB7 in cosolvent–water mixtures

The fluorescence intensity (I) growth was monitored upon 1:1 mixing of equimolar Pal and CB7 solutions containing identical cosolvent concentrations to follow the association kinetics. As a representative example, Fig. 4A depicts the kinetic traces at different DMSO concentrations. The corresponding results for the other cosolvents are presented in Figs. S20-S22 in the Supplementary data). The initial growth in intensity decelerated upon gradual addition of DMSO or MF, and the reduced plateau signals indicated that competitive binding of the cosolvent to CB7 lowered the amount of Pal–CB7 in the equilibrium. To obtain the apparent rate constants (k_{in}), the numerical solutions of the differential equation describing the reversible binding equilibrium were fitted to the experimental signals while keeping the previously determined k_{out} values constant:

$$\frac{\mathrm{d}I}{\mathrm{d}t} = \alpha\frac{\mathrm{d[Pal{-}CB7]}}{\mathrm{d}t} = \alpha(k_{\mathrm{in}}[\mathrm{Pal}][\mathrm{CB7}] - k_{\mathrm{out}}[\mathrm{Pal} - \mathrm{CB7}]) \quad (11)$$

where t denotes time, and α is a proportionality constant. The calculated k_{in} values decreased with increasing DMSO or MF concentration (Fig. 4B), indicating that both the acceleration of Pal–CB7 dissociation and the slowdown of its formation contribute to the reduced binding affinity in the presence of these cosolvents. The results of analogous experiments showed that DMF markedly enhanced k_{in}, whereas AN had little effect.

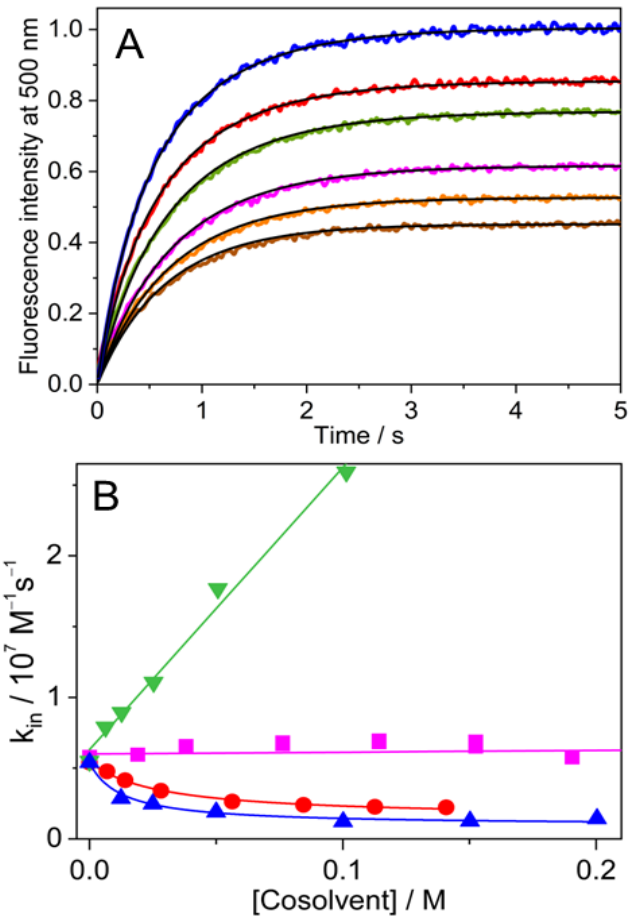

394 **Figure 4** (A) Time-dependent increase in fluorescence intensity in the presence of 0, 7, 28, 56,
395 84, and 110 mM DMSO (from top to bottom) after mixing equimolar Pal and CB7 solutions.
396 Excitation occurred at 340 nm, [Pal] = [CB7] = 0.25 μM at t = 0 s. (B) Rate constants for Pal
397 entry into CB7 as a function of cosolvent concentration in water at 298 K. DMF (▼), AN (■),
398 DMSO (●), and MF (▲).

399

400 **4. Discussion**

401 Our results demonstrates that even ~1 vol% organic cosolvents can strongly modulate the
402 thermodynamics and kinetics of reversible host-guest binding. The correlation between the
403 enthalpy and entropy values of complexation was very poor. Although all cosolvents studied
404 showed enthalpy-driven interactions with CB7, the strongest driving force was observed for
405 DMF, which is attributed to the substantial entropy gain associated with its complexation (Table
406 1). At concentrations below 40 vol%, DMF is incorporated into the hydrogen bond network of

water by forming hydrogen bonds stronger than those between water molecules themselves [37, 58]. A previous study revealed that, on average, 1.9 water molecules remain in CB7 after the confinement of DMF [59]. The DMF packing coefficient of 31% (Table 1) also indicates that DMF fits only loosely within the CB7 cavity. Consequently, its transfer from the hydrogen-bonded solvent network to the macrocycle interior leads to enhanced configurational freedom. Furthermore, the partial expulsion of the high-energy water molecules from the hydrophobic core of the host also contributes to the substantial entropy gain in the formation of the DMF–CB7 complex. In contrast, the other cosolvents do not reinforce the water structure. Therefore, their transfer from the bulk solution into CB7 leads to an entropy loss that diminishes their binding affinity. The K_{CS} values listed in Table 1 should be considered as apparent binding constants, as they were determined under varying cosolvent concentrations, where the observed equilibria reflect not only incorporation into CB7 but also concomitant alterations in the solvent structure. A parallel increase was observed (Table1) between the K_{CS} values and the packing coefficients (PC) introduced by Rebek and Mecozzi for molecular capsules [50]. The low affinity of the cosolvent to CB7 is consistent with previous findings indicating that optimal immersion occurs when the PC is within the range of 0.55±0.09 [50], whereas substantially smaller values are associated with weakened encapsulation propensity [49, 60]. Although steric compatibility is not the sole factor influencing the strength of guest-CB7 association [61, 62], the PC values suggest that two AN molecules can be accommodated within the CB7, while the inclusion of only a single DMF, DMSO or MF is likely, in agreement with the calorimetric titration results. Molecular dynamics calculations confirmed the 1:1 binding of DMF and DMSO at the equatorial region of CB7 and the retention of residual water within the cavity [63]. NMR spectra verified the deep insertion of the cosolvents into this cavitand; however, 1:1 complexation was assumed for all guests [26], in contrast to our ITC results demonstrating the incorporation of two AN molecules into CB7.

Previous density functional theory (DFT) calculations showed that Pal is only partially included within the CB7 cavity, as the alkaloid is considerably longer than the height of the host. The isoquinoline moiety is encapsulated, with its heterocyclic nitrogen positioned near one of the carbonyl-laced portals of the macrocycle [54]. In 0.2 M DMF aqueous solution, Pal–CB7 complex formation was accompanied by an unfavorable entropy change (ΔS, Table 3). This behavior arises because the configurational restriction imposed by the host–guest association cannot be overbalanced by the entropy benefit stemming from solvent removal from CB7 and the solvate shells of the reactants, as the released molecules readily integrate into the bulk hydrogen bond network. In contrast, the other cosolvents promoted entropy gain. In the presence of DMSO or MF, which disrupts the hydrogen-bonded structure of water [39, 40], the liberated solvent molecules cannot be incorporated into an extended hydrogen bond network. As a result, Pal–CB7 complex formation in these cosolvent-containing solutions was accompanied by a significant entropy increase. In the dilute AN solution used here, the water structure was only slightly perturbed [38]. Consequently, the substantial increase in ΔS (Table 3) is primarily due to the release of solvent molecules from both the CB7 cavity and the solvation sphere of Pal. Density functional theory (DFT) calculations have revealed that quinolinium cations interact more strongly with AN than with water [64]. A similar preferential solvation effect is likely operative for Pal, a structurally related isoquinolinium alkaloid. Consequently, the liberation of AN molecules from the solvation shell of Pal contributes significantly to the observed entropy gain (ΔS).

The inclusion of Pal in CB7 is less exothermic in cosolvent-containing solutions than in water (Table 3), where the pronounced enthalpy gain mainly stems from the displacement of high-energy water molecules from the hydrophobic core of CB7 [59, 65, 66]. Cosolvents diminish the number of water molecules bound to the cavity, thereby lowering the enthalpy gain upon Pal encapsulation. For example, after the inclusion of DMSO or DMF, on average, only

two water molecules remain in CB7 [59]. In addition, the energy required to release cosolvents from CB7 ($-\Delta H_{CS}$ in Table 1) further decreases the overall enthalpy benefit related to Pal–CB7 formation (ΔH). The most negative ΔH was observed in the presence of DMF, as these cosolvent molecules are incorporated into the extended hydrogen-bonded network of bulk solvent after its release from CB7. This energetically favorable process makes ΔH more negative compared to cosolvents that cannot be integrated into the water-structure.

Cosolvents reduce the temperature dependence of the Pal–CB7 binding constant compared to that in pure water as can be inferred from the ΔH and ΔS values summarized in Table 3. For example, increasing the temperature from 298 K to 303 K results in a 14.1, 14.6, 17.0, 19.0, and 21.8 % decrease in the Pal–CB7 binding constant in 0.2 M AN, DMSO, MF, DMF aqueous solutions, and in pure water, respectively

The cosolvent effects observed for Pal–CB7 complexation differ fundamentally from those reported for other host–guest systems. Alcohols influenced fluasterone encapsulation in 2-hydroxypropyl-β-cyclodextrin (HPβCD) through competitive binding to both the host and the fluasterone–HPβCD complex [67]. In triglycine–18-crown-6 binding, DMSO enhanced both the binding constant and the exothermicity of complexation, while simultaneously inducing a strongly endothermic change in host solvation [68]. When the more weakly solvated [2.2.2]cryptand was employed as the host, DMSO below 0.2 mole fraction (10.98 M) produced a smaller increase in binding constant while leaving the enthalpy gain of the complexation essentially unchanged [69]. The binding affinity of benzoate anion to HPβCD was only slightly reduced at 0.1 mole fraction (5.49 M) DMSO, owing to the minor enthalpy change of complexation [21]. The addition of 5 vol% (0.70 M) DMSO resulted in a marked entropy loss for tetraethylammonium cation inclusion in the tetrahedral $[M_4L_6]^{12-}$ metal–ligand nanocages [70]. These diverse differences demonstrate that cosolvent effects on the enthalpy–entropy

balance of host–guest association are highly system-specific, with Pal–CB7 complexation being perturbed by far lower cosolvent concentrations than in previously reported systems.

Fig. 5 illustrates the contribution of the enthalpy change of Pal–CB7 dissociation to the activation enthalpy of this process ($\Delta H^{\ddagger}_{\mathrm{out}}$) in water and in 0.2 M aqueous cosolvent solutions.

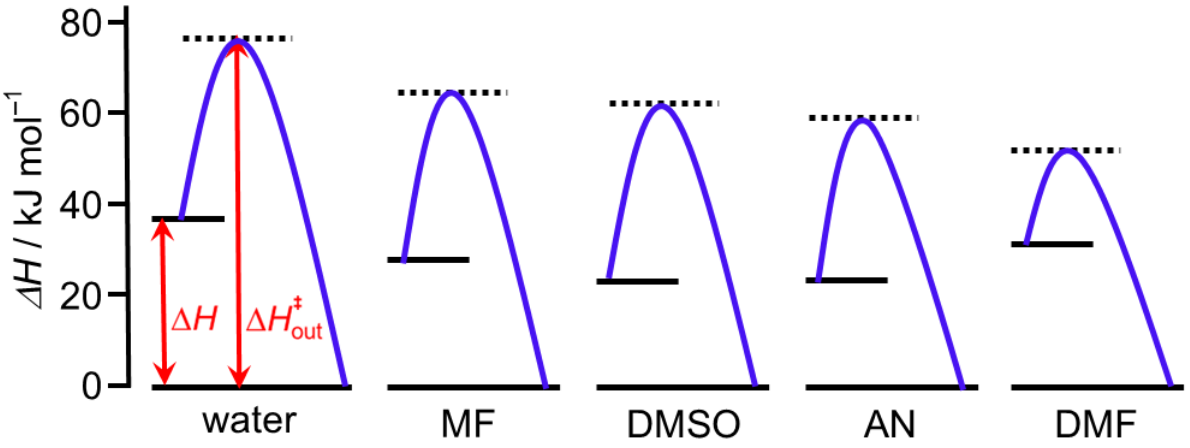

Fig. 5 Energy level diagrams for Pal complexation with CB7 in water and in 0.2 M cosolvent aqueous solution. Dotted lines represent the energy levels of the transition states.

There was no correlation between these two quantities. All cosolvents reduced $\Delta H^{\ddagger}_{\mathrm{out}}$ compared to water, irrespective of their influence on ΔH. The partial release of Pal from CB7 along the pathway to the transition state increases the hydrophobic surface exposed to the solvent, around which the hydrogen bond network becomes energetically suboptimal. This hydrophobic hydration is strongly endothermic in neat water, but organic cosolvents mitigate the energetic frustration of the water molecules surrounding the hydrophobic part of the activated complex, leading to lower $\Delta H^{\ddagger}_{\mathrm{out}}$. As shown in Table 3, the marked decline in $\Delta H^{\ddagger}_{\mathrm{out}}$ is responsible for the accelerated dissociation of the Pal–CB7 complex in cosolvent-containing media. However, this effect is partially offset by the concomitant decrease in activation entropy ($\Delta S^{\ddagger}_{\mathrm{out}}$). In neat water, Pal egression exhibits a negligible $\Delta S^{\ddagger}_{\mathrm{out}}$ (Table 3), as the growing configurational freedom on approaching the transition state counterbalances the entropy loss caused by the simultaneous

ordering of water in the hydrate shell. In contrast, the addition of cosolvent results in strongly negative $\Delta S^{\ddagger}_{\mathrm{out}}$ values, indicating a more ordered transition state than in neat water. The strongest effect was found in the presence of DMF, which readily binds to the hydrogen bond network surrounding the activated complex. In contrast, the other cosolvents show looser coordination in the transition state, yielding less unfavorable $\Delta S^{\ddagger}_{\mathrm{out}}$ values.

The determined kinetic parameter for Pal ingression into CB7, k_{in}, is an apparent rate constant, as it is influenced by the decrease in the free CB7 concentration resulting from cosolvent–CB7 interaction. This effect cannot be separated because the measurable binding constant of this complexation (K_{CS}) is an overall quantity. The cosolvent concentration dependent intrinsic binding constant cannot be determined. Nevertheless, k_{in} is useful for assessing the influence of the cosolvents on the overall rate of Pal–CB7 complex formation. At 298 K, the $k_{\mathrm{in}}/k_{\mathrm{out}}$ values agreed with the binding constants (K) obtained from independent experiments (Table 3). The considerable increase in k_{in} upon addition of DMF (Fig. 4B) is in accordance with the smallest enthalpy barrier ($\Delta H^{\ddagger}_{\mathrm{out}} + \Delta H$) observed for the Pal association with CB7 in this solvent mixture (Fig. 5). In the presence of the other cosolvents, this enthalpy barrier is similar to that in neat water. The minor changes in k_{in} stem from the combined influences of the enthalpic variation and the structural ordering of the activated complex.

The influence of cosolvents on the egression rate constant of the CB7-bound Pal (k_{out}) is similar to that reported for guest release triggered by metal cations [71, 72]. Nevertheless, the linear increase in k_{out} with cosolvent concentration argues against ternary Pal–CB7–cosolvent complex formation, as involvement of such a complex would cause k_{out} to approach a plateau [71]. The bimolecular expulsion of Pal from the CB7 cavity by cosolvent would be consistent with the linear rise of k_{out} with cosolvent concentration, but the stopped-flow data collected under different initial conditions could not be adequately rationalized when this reaction step was incorporated into the kinetic model. Only the combined effects of cosolvent-induced

variation of the solvent structure and cosolvent–CB7 complex formation can account for all experimental observations.

5. Conclusions

Our results highlight the pivotal role of cosolvent-induced changes in water-structure and solvation shell in governing both the binding affinity and the kinetics of reversible guest inclusion within the CB7 cavity. Dissociation rate measurements revealed that cosolvents not only compete for CB7 binding but also accelerate guest release by reducing the activation parameters of complex dissociation. The water-structure-enhancing DMF substantially enhanced the rate of Pal–CB7 complex formation, whereas water-structure-disrupting cosolvents decelerated the process. Cosolvent addition weakened the Pal–CB7 binding affinity by diminishing the enthalpy gain of complexation, with DMF additionally causing unfavorable entropic contribution. Cosolvent confinement in CB7 was consistently exothermic, but only DMF encapsulation was coupled with an entropy increase, resulting in the highest binding constant among the produced cosolvent–CB7 complexes. The elucidated distinct effects provide deeper mechanistic insight into the relationship between cosolvent properties and their influence on host–guest complexation, enabling the prediction of cosolvent-mediated changes in kinetic and thermodynamic behavior. This knowledge is crucial for the rational design of macrocycle-based self-assembled systems and for tailoring supramolecular interactions in applications such as drug delivery, molecular sensing, and functional molecular devices.

Acknowledgement

This work was supported by National Research, Development and Innovation Office – NKFIH, grant number K142139.

Appendix A. Supplementary data

Supplementary data to this article can be found online at

References

[1] J.S. Trivedi, Z. Yue, Solubilization using cosolvent approach, Water-insoluble drug formulation, CRC Press, Boca Raton, 2018, pp. 177–209, https://doi.org/10.1201/9781315120492.

[2] R.G. Strickley, Solubilizing excipients in oral and injectable formulations, Pharm. Res. 21 (2004) 201–230, https://doi.org/10.1023/B:PHAM.0000016235.32639.23.

[3] G. Chen, E.E. Dormidontova, Cosolvent-induced gating and structural changes in poly(ethylene oxide)-grafted gold nanopores, Macromolecules 57 (2024) 434–444, https://doi.org/10.1021/acs.macromol.3c02053.

[4] D.Y. Zhang, A.J. Schwendinger, M.A. Calabrese, Dimethylformamide-mediated polymer microstructure dictates the extensional rheology of aqueous PNIPAM solutions, Macromolecules 57 (2024) 9109–9120, https://doi.org/10.1021/acs.macromol.4c01658.

[5] G. Reddy, A.N. Muttathukattil, B. Mondal, Cosolvent effects on the growth of amyloid fibrils, Curr. Opin. Struct. Biol. 60 (2020) 101–109, https://doi.org/10.1016/j.sbi.2019.12.011.

[6] A. Nandakumar, Y. Ito, M. Ueda, Solvent effects on the self-assembly of an amphiphilic polypeptide incorporating α-helical hydrophobic blocks, J. Am. Chem. Soc. 142 (2020) 20994–21003, https://doi.org/10.1021/jacs.0c03425.

[7] L. Ostermeier, R. Oliva, R. Winter, The multifaceted effects of DMSO and high hydrostatic pressure on the kinetic constants of hydrolysis reactions catalyzed by α-chymotrypsin, Phys. Chem. Chem. Phys. 22 (2020) 16325–16333, https://doi.org/10.1039/D0CP03062G.

[8] C. Held, T. Stolzke, M. Knierbein, M.W. Jaworek, T.Q. Luong, R. Winter, G. Sadowski, Cosolvent and pressure effects on enzyme-catalysed hydrolysis reactions, Biophys. Chem. 252 (2019) 106209, https://doi.org/10.1016/j.bpc.2019.106209.

[9] T. Chang, G. Li, D. Chang, R. Amini, X. Zhu, T. Zhao, J. Gu, Z. Li, Y. Li, An RNA-cleaving DNAzyme that requires an organic solvent to function, Angew. Chem. Int. Ed. 62 (2023) e202310941, https://doi.org/10.1002/anie.202310941.

[10] A. Ramesh, T.N. Das, T.K. Maji, G. Ghosh, Unravelling denaturation, temperature and cosolvent-driven chiroptical switching in peptide self-assembly with switchable piezoelectric responses, Chem. Sci. 15 (2024) 16355–16366, https://doi.org/10.1039/D4SC05016A.

[11] J.-G. Jia, C.-C. Zhao, Y.-F. Wei, Z.-M. Zhai, S.-S. Bao, A.J. Jacobson, J. Ma, L.-M. Zheng, Macroscopic helical assembly of one-dimensional coordination polymers: helicity inversion triggered by solvent isomerism, J. Am. Chem. Soc. 145 (2023) 23948–23962, https://doi.org/10.1021/jacs.3c05552.

[12] J. Wang, K. Liu, L. Yan, A. Wang, S. Bai, X. Yan, Trace solvent as a predominant factor to tune dipeptide self-assembly, ACS Nano 10 (2016) 2138–2143, https://doi.org/10.1021/acsnano.5b06567.

[13] F.-Y. Chen, R. Fu, Z. Gong, C. Li, D.-S. Guo, K. Cai, Ultrahigh-affinity molecular recognition in water and biomedical applications, Angew. Chem. Int. Ed. 64 (2025) e202500916, https://doi.org/10.1002/anie.202500916.

[14] J. Krämer, R. Kang, L.M. Grimm, L. De Cola, P. Picchetti, F. Biedermann, Molecular probes, chemosensors, and nanosensors for optical detection of biorelevant molecules and ions in aqueous media and biofluids, Chem. Rev. 122 (2022) 3459–3636, https://doi.org/10.1021/acs.chemrev.1c00746.

[15] C. Wang, L. Xu, Z. Jia, T.-P. Loh, Recent applications of macrocycles in supramolecular catalysis, Chin. Chem. Lett. 35 (2024) 109075, https://doi.org/10.1016/j.cclet.2023.109075.

598 [16] Y.C. Yu Liu, Heng-Yi Zhang, Handbook of macrocyclic supramolecular assembly,
599 Springer, Singapore, 2020, https://doi.org/10.1007/978-981-13-1744-6.
600 [17] Z. Li, Y.-W. Yang, Macrocycle-based porous organic polymers for separation, sensing, and
601 catalysis, Adv. Mater. 34 (2022) 2107401, https://doi.org/10.1002/adma.202107401.
602 [18] M. Kfoury, C. Geagea, S. Ruellan, H. Greige-Gerges, S. Fourmentin, Effect of cyclodextrin
603 and cosolvent on the solubility and antioxidant activity of caffeic acid, Food Chem. 278 (2019)
604 163–169, https://doi.org/10.1016/j.foodchem.2018.11.055.
605 [19] L. Nakhle, M. Kfoury, H. Greige-Gerges, S. Fourmentin, Effect of dimethylsulfoxide,
606 ethanol, α- and β-cyclodextrins and their association on the solubility of natural bioactive
607 compounds, J. Mol. Liq. 310 (2020) 113156, https://doi.org/10.1016/j.molliq.2020.113156.
608 [20] C. Cai, M. Liu, H. Yan, Y. Zhao, Y. Shi, Q. Guo, W. Pei, J. Han, Z. Wang, A combined
609 calorimetric, spectroscopic and molecular dynamic simulation study on the inclusion
610 complexation of (E)-piceatannol with hydroxypropyl-β-cyclodextrin in various alcohol + water
611 cosolvents, J. Chem. Thermodyn. 132 (2019) 341–351,
612 https://doi.org/10.1016/j.jct.2019.01.009.
613 [21] T.R. Usacheva, D.A. Alister, N.N. Kuranova, V.A. Volynkin, D.A. Lindt, L.T. Pham, F.
614 D'Aria, C. Giancola, Effect of water-dimethyl sulfoxide solvents on thermodynamic parameters
615 of complex formation between benzoic acid and 2-hydroxypropyl-β-cyclodextrin, J. Therm.
616 Anal. Calorim. 149 (2024) 12325–12333, https://doi.org/10.1007/s10973-024-13534-5.
617 [22] T. Lan Pham, T.R. Usacheva, D.A. Alister, T. Thu Ha Nguyen, N.V. Tukumova, N.N.
618 Kuranova, X. Minh Vu, T. My Hanh Le, Q. Tung Nguyen, D. Lam Tran, Thermodynamic
619 parameters and quantum chemical calculations of complex formation between rutin and 2-
620 hydroxypropyl-β-cyclodextrin in water-ethanol solvents, J. Mol. Liq. 366 (2022) 120324,
621 https://doi.org/10.1016/j.molliq.2022.120324.

[23] D.L. Isac, P. Tîrnovan, A. Nicolescu, A. Fifere, A. Neamtu, M. Pinteala, Cosolvent effects on the complexation of the antifungal propiconazole nitrate with β-cyclodextrin: A combined molecular dynamics and NMR study, Eur. J. Pharm. Sci. 213 (2025) 107248, https://doi.org/10.1016/j.ejps.2025.107248.

[24] K. Kim, J. Murray, S. Narayanan, Y.H. Ko, I. Hwang, Cucurbiturils: Chemistry, Supramolecular Chemistry And Applications, World Scientific Publishing Company2018, https://books.google.hu/books?id=5CljDwAAQBAJ.

[25] D. Das, K.I. Assaf, W.M. Nau, Applications of cucurbiturils in medicinal chemistry and chemical biology, Front. Chem. 7 (2019) 619, https://doi.org/10.3389/fchem.2019.00619.

[26] I.W. Wyman, D.H. Macartney, Cucurbit[7]uril host-guest complexes with small polar organic guests in aqueous solution, Org. Biomol. Chem. 6 (2008) 1796–1801, https://doi.org/10.1039/B801650J.

[27] C. Li, J. Li, X. Jia, Selective binding and highly sensitive fluorescent sensor of palmatine and dehydrocorydaline alkaloids by cucurbit[7]uril, Org. Biomol. Chem. 7 (2009) 2699–2703, https://doi.org/10.1039/B820852B.

[28] A. Buczkowski, P. Tokarz, B. Palecz, Thermodynamic study of ethanol impact on gemcitabine binding to cucurbit[7]uril in aqueous solutions, J. Chem. Thermodyn. 153 (2021) 106317, https://doi.org/10.1016/j.jct.2020.106317.

[29] Y. Liu, C.-J. Li, D.-S. Guo, Z.-H. Pan, Z. Li, A comparative study of complexation of β-cyclodextrin, calix[4]arenesulfonate and cucurbit[7]uril with dye guests: fluorescence behavior and binding ability, Supramol. Chem. 19 (2007) 517–523, https://doi.org/10.1080/10610270601145444.

[30] R. Andrýs, A. Klusoňová, M. Lísa, J. Žd'árová Karasová, Encapsulation of oxime acetylcholinesterase reactivators: influence of physiological conditions on the stability of

oxime-cucurbit[7]uril complexes, New J. Chem. 44 (2020) 14367–14372, https://doi.org/10.1039/D0NJ03102J.

[31] K. Kotturi, E. Masson, Directional self-sorting with cucurbit[8]uril controlled by allosteric π–π and metal–metal interactions, Chem. Eur. J. 24 (2018) 8670–8678, https://doi.org/10.1002/chem.201800856.

[32] D. Lončarić, F. Movahedifar, J.R. Štoček, M. Dračínský, J. Cvačka, S. Guan, B.J. Bythell, I. Císařová, E. Masson, J. Kaleta, Solvent-controlled formation of alkali and alkali-earth-secured cucurbituril/guest trimers, Chem. Sci. 14 (2023) 9258–9266, https://doi.org/10.1039/D3SC02032K.

[33] K. Moon, A.E. Kaifer, Modes of binding interaction between viologen guests and the cucurbit[7]uril host, Org. Lett. 6 (2004) 185–188, https://doi.org/10.1021/ol035967x.

[34] A. Thangavel, A.M.M. Rawashdeh, C. Sotiriou-Leventis, N. Leventis, Simultaneous electron transfer from free and intercalated 4-benzoylpyridinium cations in cucurbit[7]uril, Org. Lett. 11 (2009) 1595–1598, https://doi.org/10.1021/ol9002459.

[35] W. Wang, A.E. Kaifer, Transfer of cationic cucurbit[7]uril inclusion complexes from water to non-aqueous solvents, Supramol. Chem. 22 (2010) 710–716, https://doi.org/10.1080/10610278.2010.500729.

[36] S. Senler, B. Cheng, A.E. Kaifer, Rotaxane formation by cucurbit[7]uril in water and DMSO solutions, Org. Lett. 16 (2014) 5834–5837, https://doi.org/10.1021/ol502479k.

[37] B. Yang, H. Lang, Z. Liu, S. Wang, Z. Men, C. Sun, Three stages of hydrogen bonding network in DMF-water binary solution, J. Mol. Liq. 324 (2021) 114996, https://doi.org/10.1016/j.molliq.2020.114996.

[38] J.E. Bertie, Z. Lan, Liquid water−acetonitrile mixtures at 25 °C: The hydrogen-bonded structure studied through infrared absolute integrated absorption intensities, J. Phys. Chem. B 101 (1997) 4111–4119, https://doi.org/10.1021/jp9639511.

671 [39] K.-I. Oh, K. Rajesh, J.F. Stanton, C.R. Baiz, Quantifying hydrogen-bond populations in
672 dimethyl sulfoxide/water mixtures, Angew. Chem. Int. Ed. 56 (2017) 11375–11379,
673 https://doi.org/10.1002/anie.201704162.
674 [40] F. Hammami, A. Chebaane, M. Bahri, S. Nasr, Structural investigations of N-
675 methylformamide-water mixtures at various concentrations, Eur. Phys. J. E 36 (2013) 129,
676 https://doi.org/10.1140/epje/i2013-13129-5.
677 [41] M. Kaczor-Kamińska, K. Kaszuba, A. Bilska-Wilkosz, M. Iciek, M. Wróbel, K. Kamiński,
678 Dimethyl sulfoxide (DMSO) as a potential source of interference in research related to sulfur
679 metabolism—a preliminary study, Antioxidants 13 (2024) 582, https://www.mdpi.com/2076-
680 3921/13/5/582.
681 [42] M. Awan, I. Buriak, R. Fleck, B. Fuller, A. Goltsev, J. Kerby, M. Lowdell, P. Mericka, A.
682 Petrenko, Y. Petrenko, O. Rogulska, A. Stolzing, G.N. Stacey, Dimethyl sulfoxide: a central
683 player since the dawn of cryobiology, is efficacy balanced by toxicity?, Regen. Med. 15 (2020)
684 1463–1491, https://doi.org/10.2217/rme-2019-0145.
685 [43] B. Valeur, Molecular fluorescence, principles and applications, Wiley-VCH, Weinheim,
686 2002, https://doi.org/10.1002/3527600248.
687 [44] W.H. Melhuish, Quantum efficiencies of fluorescence of organic substances: effect of
688 solvent and concentration of the fluorescent solute, J. Phys. Chem. 65 (1961) 229–235,
689 https://doi.org/10.1021/j100820a009.
690 [45] D. Qiu, J. Tang, S. Li, Q. Zhai, Y. Jiang, M. Hu, Solubility, density and refractive index of
691 formamide/N-methylformamide/N, N-dimethylformamide + Rb2SO4 + H2O ternary systems
692 at 283.2, 298.2 and 313.2 K, J. Chem. Thermodyn. 175 (2022) 106907,
693 https://doi.org/10.1016/j.jct.2022.106907.

694 [46] R.G. LeBel, D.A.I. Goring, Density, viscosity, refractive index, and hygroscopicity of
695 mixtures of water and dimethyl sulfoxide, J. Chem. Eng. Data 7 (1962) 100–101,
696 https://doi.org/10.1021/je60012a032.
697 [47] V. Campos, A.C. Gómez Marigliano, H.N. Sólimo, Density, viscosity, refractive index,
698 excess molar volume, viscosity, and refractive index deviations and their correlations for the
699 (formamide + water) system. isobaric (vapor + liquid) equilibrium at 2.5 kPa, J. Chem. Eng.
700 Data 53 (2008) 211–216, https://doi.org/10.1021/je700517f.
701 [48] L. Mandić, I. Džeba, D. Jadreško, B. Mihaljević, L. Biczók, N. Basarić, Photophysical
702 properties and electron transfer photochemical reactivity of substituted phthalimides, New J.
703 Chem. 44 (2020) 17252–17266, https://doi.org/10.1039/D0NJ03465G.
704 [49] W.M. Nau, M. Florea, K.I. Assaf, Deep inside cucurbiturils: Physical properties and
705 volumes of their inner cavity determine the hydrophobic driving force for host–guest
706 complexation, Isr. J. Chem. 51 (2011) 559–577, http://dx.doi.org/10.1002/ijch.201100044.
707 [50] S. Mecozzi, J. Rebek, Julius, The 55 % solution: A formula for molecular recognition in
708 the liquid state, Chem. Eur. J. 4 (1998) 1016–1022, https://doi.org/10.1002/(SICI)1521-
709 3765(19980615)4:6<1016::AID-CHEM1016>3.0.CO;2-B.
710 [51] Y.-q. Wang, Q.-y. Li, M. Jiang, X. Yang, X. Wu, X. Yu, L. Xu, A palmatine-based
711 fluorescent sensor for sensitive fluorometric and smartphone-assisted on-site fluorescent
712 colorimetric detection of water in organic solvents, Microchem. J. 179 (2022) 107598,
713 https://doi.org/10.1016/j.microc.2022.107598.
714 [52] L. Li, W.-C. Luo, M. Jiang, X. Yu, L. Xu, Turn-on fluorescence probing of amyloid fibrils
715 by the proto-berberine alkaloids and the study of their interactions, Int. J. Biol. Macromol. 231
716 (2023) 123319, https://doi.org/10.1016/j.ijbiomac.2023.123319.
717 [53] P.-H. Shan, J. Zhao, X.-Y. Deng, R.-L. Lin, B. Bian, Z. Tao, X. Xiao, J.-X. Liu, Selective
718 recognition and determination of phenylalanine by a fluorescent probe based on cucurbit[8]uril

719 and palmatine, Anal. Chim. Acta 1104 (2020) 164–171,
720 https://doi.org/10.1016/j.aca.2020.01.007.
721 [54] Z. Miskolczy, L. Biczók, G. Lendvay, Substituent effect on the dynamics of the inclusion
722 complex formation between protoberberine alkaloids and cucurbit[7]uril, Phys. Chem. Chem.
723 Phys. 20 (2018) 15986–15994, https://doi.org/10.1039/C8CP01845F.
724 [55] S.J. Strickler, R.A. Berg, Relationship between absorption intensity and fluorescence
725 lifetime of molecules, J. Chem. Phys. 37 (1962) 814–822, https://doi.org/10.1063/1.1733166.
726 [56] Z. Miskolczy, L. Biczók, I. Jablonkai, Kinetics of the reversible inclusion of flavopereirine
727 in cucurbit[7]uril, Phys. Chem. Chem. Phys. 19 (2017) 766–773,
728 http://doi.org/10.1039/C6CP07553C.
729 [57] Z. Miskolczy, M. Megyesi, O. Toke, L. Biczók, Change of the kinetics of inclusion in
730 cucurbit[7]uril upon hydrogenation and methylation of palmatine, Phys. Chem. Chem. Phys.
731 21 (2019) 4912–4919, https://doi.org/10.1039/C8CP07231K.
732 [58] X. Liu, S. Wang, X. Xu, H. Khair, Z. Dong, H. Wang, W. Zhang, T. Yu, Z. Men, C. Sun, S.
733 Wang, Exploring the dynamic changes in hydrogen bond structure of water and heavy water
734 under external perturbation of DMF, Spectrochim Acta A Mol. Biomol. Spectrosc. 305 (2024)
735 123493, https://doi.org/10.1016/j.saa.2023.123493.
736 [59] F. Biedermann, V.D. Uzunova, O.A. Scherman, W.M. Nau, A. De Simone, Release of high-
737 energy water as an essential driving force for the high-affinity binding of cucurbit[n]urils, J.
738 Am. Chem. Soc. 134 (2012) 15318–15323, https://doi.org/10.1021/ja303309e.
739 [60] K.I. Assaf, W.M. Nau, Cucurbiturils: from synthesis to high-affinity binding and catalysis,
740 Chem. Soc. Rev. 44 (2015) 394–418, http://dx.doi.org/10.1039/C4CS00273C.
741 [61] K.I. Assaf, W.M. Nau, Dispersion interactions in condensed phases and inside molecular
742 containers, Acc. Chem. Res. 56 (2023) 3451–3461,
743 https://doi.org/10.1021/acs.accounts.3c00523.

744 [62] L.M. Grimm, S. Spicher, B. Tkachenko, P.R. Schreiner, S. Grimme, F. Biedermann, The
745 role of packing, dispersion, electrostatics, and solvation in high-affinity complexes of
746 cucurbit[n]urils with uncharged polar guests, Chem. Eur. J. 28 (2022) e202200529,
747 https://doi.org/10.1002/chem.202200529.
748 [63] N. Chiangraeng, H. Nakano, P. Nimmanpipug, N. Yoshida, Theoretical analysis of the role
749 of water in ligand binding to cucurbit[n]uril of different sizes, J. Phys. Chem. B 127 (2023)
750 3651–3662, https://doi.org/10.1021/acs.jpcb.3c00343.
751 [64] N.J.A. Coughlan, C. Liu, M.J. Lecours, J.L. Campbell, W.S. Hopkins, Preferential ion
752 microsolvation in mixed-modifier environments observed using differential mobility
753 spectrometry, J. Am. Soc. Mass. Spectrom. 30 (2019) 2222–2227,
754 https://doi.org/10.1007/s13361-019-02332-1.
755 [65] J. Setiadi, F. Biedermann, W.M. Nau, M.K. Gilson, Thermodynamics of water
756 displacement from binding sites and its contributions to supramolecular and biomolecular
757 affinity, Angew. Chem. Int. Ed. 64 (2025) e202505713,
758 https://doi.org/10.1002/anie.202505713.
759 [66] F. Biedermann, W.M. Nau, H.-J. Schneider, The hydrophobic effect revisited—studies with
760 supramolecular complexes imply high-energy water as a noncovalent driving force, Angew.
761 Chem. Int. Ed. 53 (2014) 11158–11171, http://doi.org/10.1002/anie.201310958.
762 [67] Y. He, P. Li, S.H. Yalkowsky, Solubilization of Fluasterone in cosolvent/cyclodextrin
763 combinations, Int. J. Pharm. 264 (2003) 25–34, https://doi.org/10.1016/S0378-5173(03)00389-
764 2.
765 [68] T.R. Usacheva, L. Pham Thi, I.V. Terekhova, R.S. Kumeev, V.A. Sharnin, Application of
766 isothermal titration calorimetry for evaluation of water–acetone and water–dimethylsulfoxide
767 solvent influence on the molecular complex formation between 18-crown-6 and triglycine at

298.15 K, J. Therm. Anal. Calorim. 121 (2015) 975–981, https://doi.org/10.1007/s10973-015-4630-0.

[69] T.R. Usacheva, L. Pham Thi, I.V. Terekhova, R.S. Kumeev, V.A. Sharnin, Thermodynamics of molecular complexation of glycyl–glycyl–glycine with cryptand [2.2.2] in water–dimethylsulfoxide solvent at 298.15 K, J. Therm. Anal. Calorim. 126 (2016) 307–314, https://doi.org/10.1007/s10973-016-5383-0.

[70] M. Nolten, K.T. Xia, S. Pezzotti, G. Schwaab, R.G. Bergman, K.N. Raymond, F. Dean Toste, T. Head-Gordon, W.-L. Li, M. Havenith, Tuning the free energy of host–guest encapsulation by cosolvent, Phys. Chem. Chem. Phys. 27 (2025) 10120–10128, http://doi.org/10.1039/D5CP00661A.

[71] Z. Miskolczy, M. Megyesi, L. Biczók, A. Prabodh, F. Biedermann, Kinetics and mechanism of cation-induced guest release from cucurbit[7]uril, Chem. Eur. J. 26 (2020) 7433–7441, https://doi.org/10.1002/chem.201905633.

[72] Z. Miskolczy, M. Megyesi, L. Biczók, Kinetics of base-promoted transformation of berberrubine-cucurbit[7]uril inclusion complex: Active role of alkali cations, J. Mol. Liq. 385 (2023) 122354, https://doi.org/10.1016/j.molliq.2023.122354.